Available online at www.jonass.ir

Journal of Nature and Spatial Sciences

Journal homepage: www.jonass.ir

Original Article

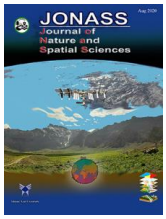

METRIC based evapotranspiration mapping of *pistachio* orchard in semi-arid region

Mohammad Hossein Mokhtari [a]*, Ibrahim Busu[b] and Sara Parvizi [c]

[a] *Department of Remote Sensing, Yazd University, Yazd, Iran*
[b] *Department of Remote Sensing, University Technology of Malaysia (UTM), Malaysia*
[c] *Department of Watershed Management Engineering, Yazd University, Yazd, Iran*

ARTICLE INFO

Article history:
Receive Date: 09 April 2021
Revise Date: 27 May 2021
Accept Date: 29 May 2021

Keywords:
Pistachio ; METRIC; Semi-arid region; Soil water balance; Evapotranspiration

ABSTRACT

Background and objective: Agricultural lands under *pistachio* crop are expanded in the Bahadoran area due to the high profitability of production. Therefore, accurate estimation of *pistachio* water requirements and efficient use of water is essential where water resources are insufficient. This study evaluates the performance of METRIC in estimating *pistachio* evapotranspiration in a semi-arid region.
Materials and methods: The satellite images utilized in this study were consisting of three clouds free LANDSAT TM5 data acquired on 28 April 2010, 17 Jul 2010, and 2 Aug 2010. These images in Tagged Image File Format were downloaded from the U.S. Geological Survey Global Visualization Viewer website. Geometric correction of images was performed by collecting 20 numbers of well-dispersed ground control points. First-order polynomial transformation with nearest neighbor resampling method was applied to each image to fit the image coordinate to the coordinate of ground control points. The accuracy of the geo-referencing was evaluated by calculation of root mean square error and it was controlled to be less than half the size of the original pixel. Then two other scenes were co-registered based on this image and a subset of interest areas was generated from image scenes. Radiometric and atmospheric calibration was performed first by converting original digital numbers to radiance.
Results and conclusion: METRIC estimates the average ET for the image on April 28, July 17 and August 2 at 2.9, 4.2 and 3.1 mm per day, respectively.

1. Introduction

Estimation of spatial and temporal variation of evapotranspiration (ET) considered as the main component of water balance, plays important role in planning and decision making in the agricultural sector (Gao and Long 2008; Gowda et al., 2008,). Crop ET is conventionally estimated from weather data recorded at the weather stations and the crop coefficient-reference ET approach. The calculation

* *Corresponding author.* Tel.: *+983531233222.*
E-mail address: mh.mokhtari@yazd.ac.ir
Peer review under responsibility of Maybod Branch, Islamic Azad University

DOI: https://dx.doi.org/10.30495/jonass.2021.1927551.1010

of the hypothetical reference crop ET (ETref) is typically performed under standard conditions, excellently managed, disease-free, large, well-watered fields, reaching a full production under the given climatic conditions. Then, empirical crop coefficient values are applied to estimate crop potential ET in different crop development stages (Allen et al., 1998). However, due to the large population of crops and fields in nature, precise estimation of crop coefficients by conventional methods is difficult (Tasumi et al., 2005). Despite the availability of several point-based ET measurement models (i.e. Penman-Monteith (PM), Priestly-Taylor, Hargreaves, Blaney–Criddle, etc.), their application in multiple scales is spatially restricted due to the wide-spread distribution of agro-climatic stations and inherent spatial heterogeneity of land surface. (Ramos et al., 2009). On the other hand, traditional estimates of actual ET require either lysimeter or water balance measurements which are costly and time-consuming (Jain et al., 2008). The capability of remote sensing techniques has been proven in providing accurate and reliable information on agricultural and hydrological condition (Gao and Long, 2008) and land surface variables such as land cover mapping, biomass estimation (Muukkonen and Heiskanen, 2005), generation of land surface temperature (Barreto, 2010), leaf area index estimation, estimation of evapotranspiration on a pixel by pixel basis and periodic information of ET using surface energy balance modeling (Gowda, et al. 2007; Ramos et al., 2009).

Several satellite-based methods including empirical direct method, inference method, residual method, and deterministic method (Choi et al., 2009) have been developed to spatially estimate ET as crop water requirement. Surface Energy Balance Algorithm for Land (SEBAL) (Bastiaanssen, et al., 1998; Jamali and Ghorbani Kalkhajeh 2020) , Surface Energy Balance System (SEBS), Simplified Surface Eenergy Balance Index (S-SEBI) (Roerink et al., 2000), Surface Energy Balance Index (SEBI), Two-Source Energy Balance (T-SEB) (Norman et al., 1995), (Su, 2002) and Hybrid model (calculates net radiation through SEBAL and surface temperature, latent heat flux and sensible heat flux from TSEB) are the residual methods that calculate energy balance component from different data sources. Most of these models solve the energy balance of land surface for latent heat flux at the satellite overpass time. Usually instantaneous ET estimated through these models are extrapolated to 24h ET and interpolated between two consecutive satellite data by means of weather data in order to estimate seasonal ET.

METRIC, Mapping Evapotranspiration at high Resolution with Internalized Calibration as a residual model is a variant of SEBAL which uses different data sources. METRIC has been applied by several researchers and proven as an efficient, accurate, and relatively cost-effective procedure for actual ET estimation (Tasumi et al., 2005; Gowda et al., 2009; Folhes et al., 2009). Similar to SEBAL, METRIC estimates actual ET from the residual part of the energy balance model, but hourly or shorter period alfalfa reference ET_{ref} is used in converting instantaneous ET to 24h rather than the evaporative fraction in SEBAL (Allen et al., 2007). Ground-based measurement of wind speed, solar radiation, air temperature, and vapor pressure as ancillary input data are required in the METRIC model. Fewer ground data requirement (solar radiation, air temperature, vapor pressure, and wind speed), automated calibration of empirical coefficient, and the use of hourly or shorter period ET_{ref} in calibration and interpolation of instantaneous ET to 24h are the advantages of the METRIC against the other methods (Allen et al., 2005; Tasumi et al. 2005; Folhes et al., 2009). In addition, extrapolation of instantaneous ET to the daily basis through ET_{ref} fraction which takes into account wind speed and air temperature, better incorporate environmental conditions particularly in the advective condition of semi-arid regions (Gowda et al., 2009; Jamali et al. 2021). The error of ET estimates via METRIC has reported to being 10 to 20% on daily basis and 1 to 4% for a seasonal estimate (Gowda et al., 2008).

In a study to estimate the evapotranspiration of an olive grove in southern Portugal, they used a metric model using Landsat images. The results show that METRIC can be used to estimate and map ET ultra-intensive olive groves with the aim of improving irrigation use and management (Pôças et al., 2014). Using the metric model to estimate evapotranspiration using Landsat satellite imagery in four different study areas in Northeast Asia, the parameters of the energy balance equation including net radiation, soil heat flux, and tangible heat flux for all study areas And evaluated and concluded that the error rate due to the use of this model to estimate the above parameters is very low.The results of the sensitivity analysis of the model showed that the choice of hot and cold pixels has a significant

effect on the accuracy of the metric model to estimate evapotranspiration (Liaqat and Choi, 2015; Qanbari and Jamali 2015).

In a study used SEBAL to estimate the water use efficiency of pistachio trees in saline conditions in Bahadoran plain. The results showed The water balance ETa estimate was 19% larger than the SEBAL based ETa due to the uncertainties involved in estimation of deep percolation and leaching fraction (Rahimian et al., 2017). A study estimated the evapotranspiration of the western part of Lake Urmia to achieve sustainable water management. In this study, an internally calibrated evapotranspiration estimation model was used to estimate monthly evapotranspiration in the period 2014-2016 using the Landsat 8 satellite. Evaluation results for ET obtained using METRIC were compared with independent ET estimation using the FAO-56 method to evaluate the accuracy of the estimate. This comparison showed a good correlation between the two types of estimation results for irrigated agriculture, which indicates the estimated success of ET in this region (Tasumi, 2019). A study comparing leaf area index (LAI), surface temperature (Ts), and actual evapotranspiration (ETa), estimated using the METRIC model based on remote sensing and in situ measurements collected during crossing The satellite landed on a cornfield in eastern South Dakota. Landsat 7 and 8 images were used for this purpose. The results showed that there is a good correlation between the variables measured in situ and estimated by the METRIC model (Reyes-González et al., 2019). In one study, they developed and tested a new ArcGIS toolbox that uses an evapotranspiration model with an internal calibration model for a semi-arid environment. The tool, named METRIC-GIS, facilitates the pre-processing operations and the automatic identification of potential calibration and pixels review. Energy balance components obtained from METRIC GIS were in conflict with those obtained from the original METRIC (Ramírez-Cuesta et al., 2020). In a study, Zhao et al. Developed a new SWH − METRIC model combining the SWH and METRIC models to simulate real daily evapotranspiration with high spatial and temporal resolution. The new model solves the ET discontinuity problem calculated by remote sensing images and hydrological models. The results showed that the simulation of the SWH - METRIC model with eddy covariance measurement, with mean R2 0.70 and root mean square error of 0.67 mm on day 1, was highly consistent and superior to the SWH model (Zhao et al., 2020).

This study is aimed at evaluating the potential of the METRIC model for mapping ET over pistachio crop in a semi-arid representative area where agricultural lands were expanded for this crop during the last decades and groundwater is extracted increasingly due to its high product profitability. Thus, there is a need for accurately quantifying the beneficial required water for this crop and increasing water use efficiency. The results of this study can be effective in water and irrigation management and the prevention of drought stress in pistachio lands.

2. Material and method

2.1. Study area

The study was conducted at the South-west of Yazd city in the Bahadoran area, the center of Iran (fig. 1). This area expands from the longitude of 54° 51′ to 54° 59′ in east and latitude of 31° 29′ to 31° 17′ in north and covers about 7000 ha. Pistachio (Pistachio vera L.) is the dominant cropping pattern in this area (over 97%) that are planted with spacing about 6m between rows and 1.70m between trees in the row. The long-term average rainfall in this area is about 71.9 mm with most of the rainfall occurring in the winter months from December to April. Monthly evaporation and mean air relative humidity is about 264 mm and 25% respectively. The water resource in this area used to be groundwater, and it is impossible to have an economical crop production without reliable irrigation. The irrigation method is conventional flooding with a frequency of 30 to 35 days which is decreased to 40 to 45 days during the autumn and winter months. The average temperature of the study area is 17.1 °C, whilst the maximum temperature in July is 41° C, and the minimum in January is -10°C. The farmlands in the village are almost flat with an average altitude of about 1500 m above

sea level. The soil types are mainly sandy loam at the top 10cm and clay loam below this depth. Fig. 1 shows the location of the study area and the position of the weather station.

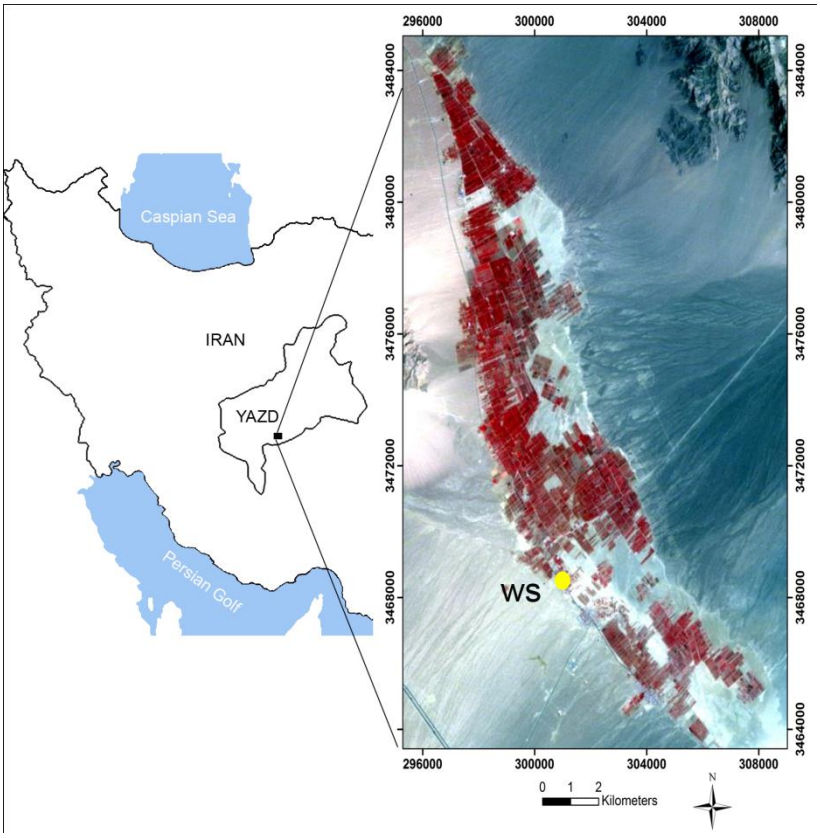

Fig. 1- Study area and the location of weather station shown on Landsat 5 TM satellite Image acquired on July 17 2010 (FCC of 4,3,2,)

2.2. Dataset and Preprocessing

The satellite images utilized in this study were consisting of three clouds free LANDSAT TM5 data (path 161, row 38) acquired on 28 April 2010, 17 Jul 2010, and 2 Aug 2010. These images in Tagged Image File Format (TIFF) were downloaded from the U.S. Geological Survey Global Visualization Viewer website (glovis.usgs.gov). Geometric correction of images was performed by collecting 20 numbers of well-dispersed ground control points (GCPs). First-order polynomial transformation with nearest neighbor resampling method was applied to each image to fit the image coordinate to the coordinate of ground control points. The accuracy of the geo-referencing was evaluated by calculation of root mean square error and it was controlled to be less than half the size of the original pixel. Then two other scenes were co-registered based on this image and a subset of interest areas was generated from image scenes. Radiometric and atmospheric calibration was performed first by converting original digital numbers to radiance using (Eq.1).

$$L = gain * DN + offset \quad (1)$$

where L is the radiance ($Wm^{-2}str\mu m$), DN is the radiometric value or digital number and gain and offset ($L_{\min}$)are calculated by the following equation.

$$gain = \frac{L_{\max} - L_{\min}}{255} \quad (2)$$

Where L_{max} and L_{min} are upper radiance limit and lower radiance limit provided by image supplier and can be found on the metadata of each dataset. For converting radiance values to the top of atmosphere reflectance in visible-near infrared and short waves bands following equation were used:

$$\rho = \frac{L_\lambda \Pi d^2}{ESUN_\lambda \cos\theta} \quad (3)$$

where $ESUN_\lambda$ is the band dependence exoatmospheric irradiance, ($Wm^{-2}str\mu m$), θ is solar zenith angle and d is the earth-sun distance (AU). In order to correct the top of the atmosphere reflectance image for scattering and absorption of incoming and outgoing, near-surface vapor pressure-based atmospheric correction was employed to convert the top of the atmosphere reflectance to at surface reflectance (Tasumi et al., 2005; Gowda et al., 2008). The Surface temperature was calculated by estimating brightness temperature as a function of the radiance of the thermal band using Eq.4. In this study, the narrow band emissivity as a function of NDVI was used to calculate surface temperature with a general atmospheric correction for the clear sky (Eq.5).

$$T_{BB} = \frac{K_2}{\ln\left(\frac{K_1}{Rad_{b6}} + 1\right)} \quad (4)$$

where K_1=607.76 and K_2=1260.56 are two constant values and Rad_{b6} is thermal band (band6) of LANDSAT image in radiance

$$T_s = \varepsilon_0^{-25} * Rad_{b6} \quad (5)$$

where T_s is the surface temperature and $\varepsilon_0$is the surface emissivity.

In addition, weather data including wind speed, radiation, maximum air temperature, minimum air temperature, vapor pressure, dew point, relative humidity with 10 minutes intervals were collected from the weather station located in the study area (Fig.1). These data were used as input for calculation of ETref from standardized ASCE Penman-Monteith equation as well as ancillary input data for METRIC model. The standardized ASCE Penman-Monteith ETref was calculated through REF-ET (V.2) software provided by the University of Idaho. For calculating soil water balance, soil water content was monitored using the TDR (Time Dominant Refloctometry) instrument. Detail of SWC measurement has been explained in Section4

2.3. Evapotranspiration with METRIC

METRIC as an extension of the SEBAL model, calculates actual Evapotranspiration (ET) from the residual part of the earth's surface energy balance on a pixel by pixel basis at satellite overpass time (Tasumi et al., 2005). A general form of energy balance is presented as eq.6.

$$LE = R_n - G - H \quad (6)$$

where LE is the latent energy (Wm^{-2}) utilized for evaporating water from the soil and transpiration from the plant ($^{mm\ day^{-1}}$), R_n (Wm^{-2}) is net radiation, G (Wm^{-2}) is soil heat flux conducted into the ground, and H (Wm^{-2}) is sensible heat flux convected into the air. A Similar approach is followed to calculate R_n and G by SEBAL and METRIC.

2.3.1. Net radiation

R_n can be partitioned into the four main components, including incoming shortwave radiation originated from the sun, a fraction of this radiation reflected by earth's surface namely outgoing shortwave, incoming longwave radiation originated from the tmosphere, and outgoing longwave radiation emitted by the earth surface.

$$R_n = R_{S\downarrow} - \alpha R_{S\downarrow} + R_{L\downarrow} - R_{L\uparrow} - (1-\varepsilon_o)R_{L\downarrow} \quad (6)$$

Where $R_{s\downarrow}$ (Wm^{-2}) is the incoming shortwave radiation that can either be measured by pyranometer in the ground station or as constant estimated at the overpass time of satellite (Eq. 8) (Allen et al. 2007), α (dimensionless) is the surface Albedo defined as the ratio of reflected solar radiation to the incident, $R_{s\downarrow}$ and $R_{l\downarrow}$ (Wm^{-2}) are the incoming and outgoing longwave radiation respectively and ε_0 is the broadband surface thermal emissivity that is calculated as function of Leaf Area Index (LAI) or Normalized Difference Vegetation Index (NDVI) as indicated in Eq.12. The term $(1-\varepsilon_0)R_{L\downarrow}$ represents the fraction of incoming longwave radiation reflected from the surface.

$$R_{S\downarrow} = \frac{G_{sc} COS\theta_{rel} \tau_{sw}}{d^2} \quad (8)$$

where θ_{rel} is the solar incidence, G_{sc} is solar constant (1367 Wm^{-2}), d^2 is square of the relative Earth–Sun distance and τ_{sw} is broad-band atmospheric transmissivity. The ratio of the incoming shortwave radiation that is reflected by the land surface is considered as outgoing shortwave radiation. It is calculated based on surface Albedo which is obtained by integrating satellite spectral reflectance's values from bands 1–5 and 7 ($\rho_1 - \rho_7$) of LANDSAT image using weighing function as shown in eq.9 (Folhes et al., 2009).

$$\alpha = 0.356\rho_1 + 0.13\rho_3 + 0.373\rho_4 + 0.085\rho_5 + 0.072\rho_7 \quad (9)$$

The outgoing long wave component of the energy balance equation is calculated as function of surface emissivity and surface temperature using the Stephan-Boltzman equation.

$$R_{L\uparrow} = \varepsilon_0 \sigma T_s^4 \quad (10)$$

Where; σ is the Stephan-Boltzman constant ($5.67*10^{-8} Wm^{-2}K^{-4}$) and T_s is the surface temperature. Metric requires satellite data that records the thermal infrared part of the spectrum in addition to visible and near-infrared wavelength. In the case of using Landsat TM5 image, it is calculated from radiance values of band 6 (Rad_6) by using the Plank equation:

$$T_s = \varepsilon_o^{-0.25} * Rad_6 \quad (11)$$

$$\varepsilon_o = 1.009 + 0.047 * LN(NDVI) \quad (12)$$

Thermal radiation emitted by the atmosphere reaches the earth's surface and it is considered as incoming longwave radiation and a component of the energy budget at the surface. $R_{L\downarrow}$ is calculated via the Stephan-Boltzman equation as follow:

$$R_{L\downarrow} = \varepsilon_a \sigma T_a^4 \quad (13)$$

where $\varepsilon_a$is air emissivity that is calculated through an empirical equation, eq. 14 (Bastiaanssen et al., 1998) and $T_a$is the air temperature in Kelvin that is measured at weather stations nearby the study area.

$$\varepsilon_a = 0.85(-LN\,\tau_{sw})^{0.09} \quad (14)$$

LAI as an indicator of canopy resistant to vapor flux is defined as the ratio of total area of one side of plant leaves to the per unit of ground area and computed as (Bastiaanssen et al., 1998):

$$LAI = -LN((0.69 - SAVI)/0.59)/0.91 \quad (15)$$

where SAVI is the Soil Adjusted Vegetation Index estimated from (Allen et al., 2007):

$$SAVI = \frac{(1+L)(\rho_4 - \rho_3)}{L + (\rho_4 + \rho_3)} \quad (16)$$

where L is the constant that often is set to 0.5 (Allen et al. 2007) and $\rho_4$and $\rho_3$are the reflectance image of Landsat TM data. An exponential function was used based on LAI measured by LI-COR, LAI 2000 instrument on the ground as shown in Eq.17. The standard error and correlation coefficient of this equation is 0.87, and 0.91 respectively. In addition, LAI was set to zero where SAVI was less than 0.065 based on ground control.

$$LAI = 21.202 * SAVI^2 - 2.905 * SAVI + 2.948 \quad (17)$$

2.3.2. Soil heat flux (G)

The amount of energy conducted into the soil is considered as soil heat flux. An empirical equation is used by METRIC for estimating soil heat flux (Bastiaanssen 2000)

$$G = (T_S - 273.15)(0.0038 + 0.0074\alpha)(1 - 0.98NDVI^4)R_n \quad (18)$$

where T_s is the surface temperature in Kelvin using thermal band, α is surface Albedo (-) and NDVI is vegetation index calculated from Red and near-infra red spectral bands. In the case of Landsat data band number 3 and 4 are used to calculate NDVI:

$$NDVI = \frac{\rho_4 - \rho_3}{\rho_4 + \rho_3} \quad (19)$$

2.3.3. Sensible heat flux (H)

The rate of heat loss to the air through convection due to temperature differences is considered as sensible heat flux. It is predicted using the difference between the surface aerodynamic temperature and a reference height air temperature (Brutsaert 1982). In both METRIC and SEBAL, the aerodynamic, temperature gradient-based equation (Eq.20) for heat transport is estimated by calculating the temperature difference between two near-surface heights.

$$H = \rho C_p \frac{dT}{r_{ah}} \tag{20}$$

where ρ is the air density kgm^{-3}, C_p is air specific heat at constant pressure (≈1004 $Jkg^{-1}k^{-1}$), and r_{ah} (sm^{-1}) is the aerodynamic resistance to heat transfer (between two near-surface height, 0.1 and 2m) which is calculated from wind speed extrapolated to some blending height above the ground surface typically 100 to 200m, and dT (k) is temperature differences in between two near-surface height.

$$r_{ah} = \frac{LN(z_2 / z_1)}{u^* k} \tag{21}$$

where z_1 and z_2 are the heights above zero plane displacement height of vegetation and u^* (ms^{-1}) is the friction velocity calculated from the logarithmic wind law for neutral atmospheric conditions and K is Von Karman's constant equal to 0.41.

$$u^* = \frac{ku_{200}}{LN(200 / z_{om})} \tag{22}$$

Where u_{200} is the wind speed at the blending height (200m, assuming wind speed is not influenced by surface roughness in this height) and z_{oom} (m) is surface roughness length for momentum transport which is defined mathematically as the plane where the wind speed becomes zero. The following equation was suggested for customizing function for z_{om} based on NDVI (Allen et al., 2007):

$$z_{om} = \exp\left[(a * NDVI / \alpha) + b\right] \tag{23}$$

Where α is the surface Albedo which is used to differentiate between tall and short vegetation with the same NDVI and a and b are regression constants derived from a plot of $LN(z_{om})$ versus $NDVI/\alpha$ for two or more circumstances in the image for specific vegetation types.

$$u_{200} = \frac{u_s * \ln(200 / zom_s)}{\ln(z_x / zom_{s)}} \tag{24}$$

where; u_s is the wind speed at the weather station at z_x height above the surface, zom_s is the surface roughness for momentum transport in the weather station. The iterative procedure is performed to calculate u. The detain information about the equation for iteration procedure can found in. Temperature differences, dT, for each pixel by assuming a linear relationship between dT and Ts estimated from satellite image thermal band.

$$dT = a + bT_S \tag{25}$$

where b and a are the calibration coefficients, and Ts is the surface temperature from the satellite. Thus, two extreme pixels namely hot and cold within the image are selected. A hot pixel is selected from bare soil close to the vegetated area and assuming the soil is enough dry as result LE is equal to zero. Consequently, the cold pixel is selected from the fully vegetated area in the image.

$$dT = \frac{(R_n - G - kET_{ref})r_{ah}}{\rho C_p} \quad (26)$$

Where ET_{ref} in (Eq. 26) is hourly reference ET that proposed to be estimated from standardized ASCE Penman–Monteith equation for alfalfa reference, k is an empirical value and is set to 1.05 by assuming 5% greater ET than the ET_{ref} in the selected field due to higher surface wetness compare to other vegetation fields, r_{ah} is aerodynamic resistant for heat transfer calculated for the hot and cold pixels, ρ is air density kgm^{-3} and c_p is air specific heat at constant pressure. Then a and b are determined iteratively using two dT value and their associated T_s values from hot and cold pixels. In order to reduce the operator dependency and error on the estimation of sensible heat flux and consequently evapotranspiration, in this study automated selection method was used to select two extremely hot and cold pixels from the image . Once R_n, H and G were calculated, eq.6

is used to estimate λE as residual of surface energy balance. Then λE is divided by latent heat of vaporization to estimate instantaneous ET at the satellite overpass time (Allen et al., 2007):

$$ET_{ins} = 3600\frac{\lambda E}{\gamma \rho_w} \quad (27)$$

where; ET_{ins} is instantaneous ET (mmh^{-1}), 3600 converts from second to hours, ρ_w is density of water (1,000 kgm^{-3})and γ is latent heat of vaporization Jkg^{-1} that is computed from:

$$\gamma = (2.501 - 0.00236(T_s - 273.15)) * 10^6 \quad (28)$$

In order to convert hourly ET to a daily basis, reference ET fraction is computed by dividing ET_{ins} to the ET_{ref} calculated from standardized ASCE Penman–Monteith equation.

$$ET_{ref}\,f = \frac{ET_{ins}}{ET_{ref}} \quad (29)$$

Finally 24h actual ET is estimated using $ET_{ref}f$ and accumulated hourly ET reference from standardized ASCE Penman–Monteith method, assuming instantaneous $ET_{ref}f$ at satellite overpass time is the same as the average $ET_{ref}f$ over the 24h (Allen et al., 2007):

$$ET_{daily} = ET_{ref}\,f \sum_{i=1}^{24} ET_{ref\,(i)} \quad (30)$$

where $\sum_{i=1}^{24} ET_{ref\,(i)}$ accumulates hourly $ET_{ref}f$ estimated from previous stage for 24h.

3. Results and discussion

The study revealed that high spatial variation of surface temperature (difference of 20 °C on April 28, 18 °C on both July 17 and Aug 2) encompasses arid and semi-arid climatic conditions in this area and as a result afternoon advective conditions is expected. Based on the ground measurement average difference of 30 to 35 °C was detected for these three days between crop canopy and bare soil at the satellite overpass time using a handheld infrared thermometer. This confirms the high variability of surface temperature. Advective condition in semi- arid area has been reported to be a source of increasing ET rate in semi arid regions (Allen et al., 2007). (Fig. 2) shows land surface heat of irrigated pistachio crop and bare soil. The areas with high and low surface temperature are associated

with bare soil and vegetated area (pistachio crop with different tree ages from 2 to 8 years old) respectively.

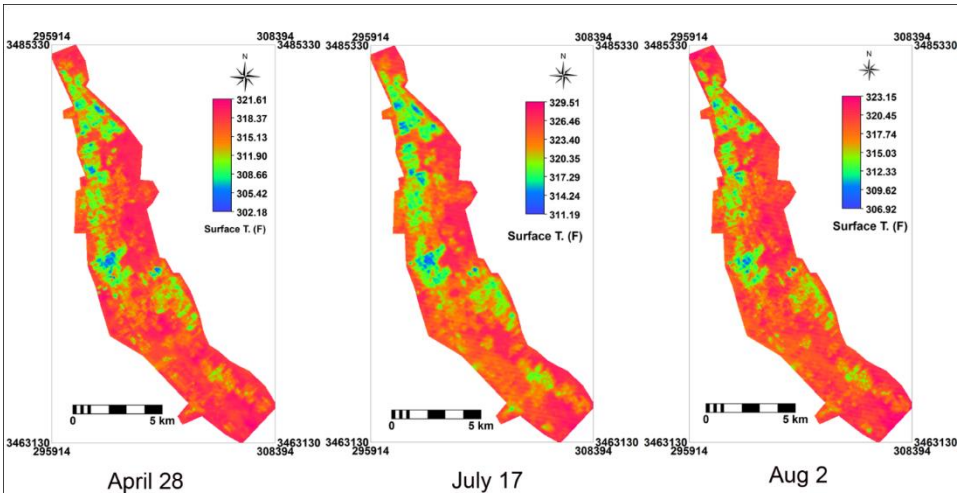

Fig.2- surface temperature estimated through Landsat image on three different data

Primary input images for the METRIC model namely NDVI, SAVI, surface Albedo, and leaf area index (LAI) that are calculated from satellite spectral bands are shown in (Fig. 3). It should be noted that 97 percent of the area is planted by pistachio crops and as a result variation in SAVI and consequently LAI map mostly corresponds to the variation of pistachio tree foliages. Besides, an area with a lower Albedo value corresponds to the high vegetation density.

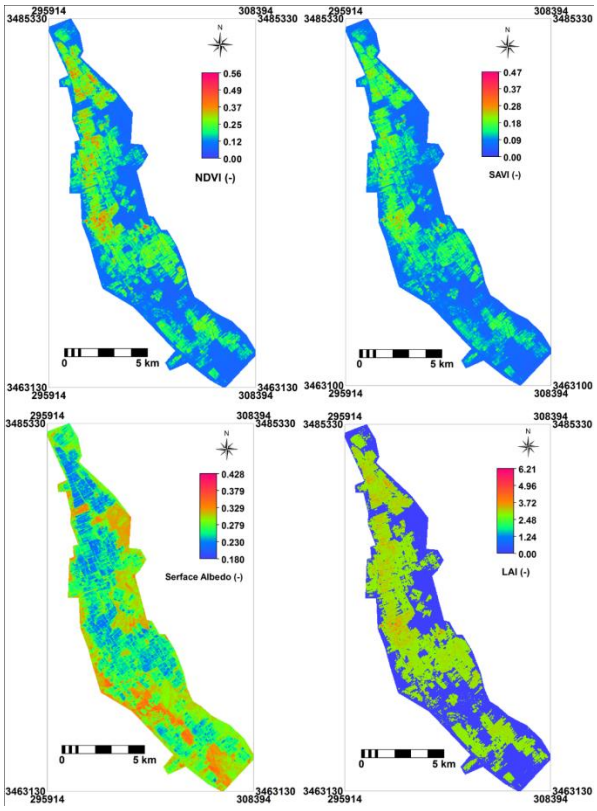

Fig. 3- primary input images of METRIC model, NDVI, SAVI, surface Albedo and LAI

The average net radiation for this area varies from 580.9 Wm^{-2} on April 28, 614 Wm^{-2}on July 17, and 622 Wm^{-2} on 2 Aug. As shown in Fig.4 higher and lower net radiation values are related to the vegetation with higher leaf area index values and bare soil respectively.

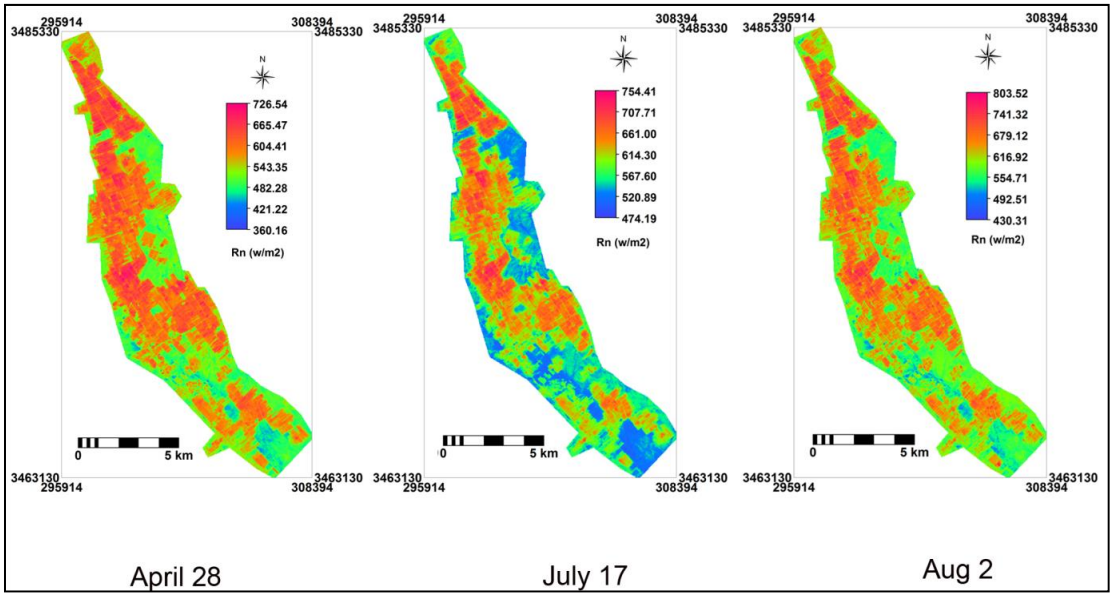

Fig.4- Net radiation map of image date April 28, July 17 and Aug 2

ET_{ref} and wind speed calculated at the daily detection and the satellite times are presented in Table 1. These values were utilized for internal calibration of METRIC and conversion from hourly ET to a daily basis. Measured wind speed at the satellite overpass time is close to the average daily wind speed on April 28 and July 17 while for the day of Aug 2 average daily wind speed is higher than the wind speed at the satellite overpass time. (Fig. 5) shows day time variability of hourly average wind speed on the image days. Daily ET maps estimated via the METRIC model are presented in Fig. 6; where red fields are the area with a high ET rate which corresponds to the area with a fully developed pistachio canopy. METRIC has an estimated average ET of 2.9, 4.2 and 3.1 mm/day for images of April 28, July 17 and August 2 respectively.

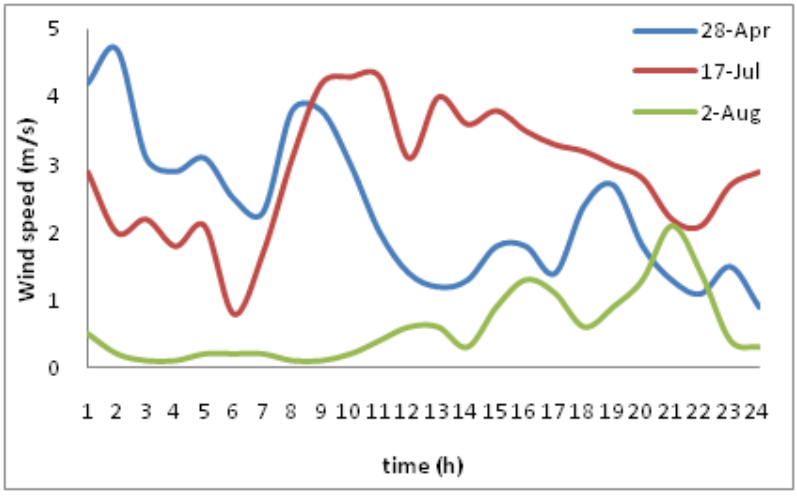

Fig. 5- day time variability of wind speed on image dates

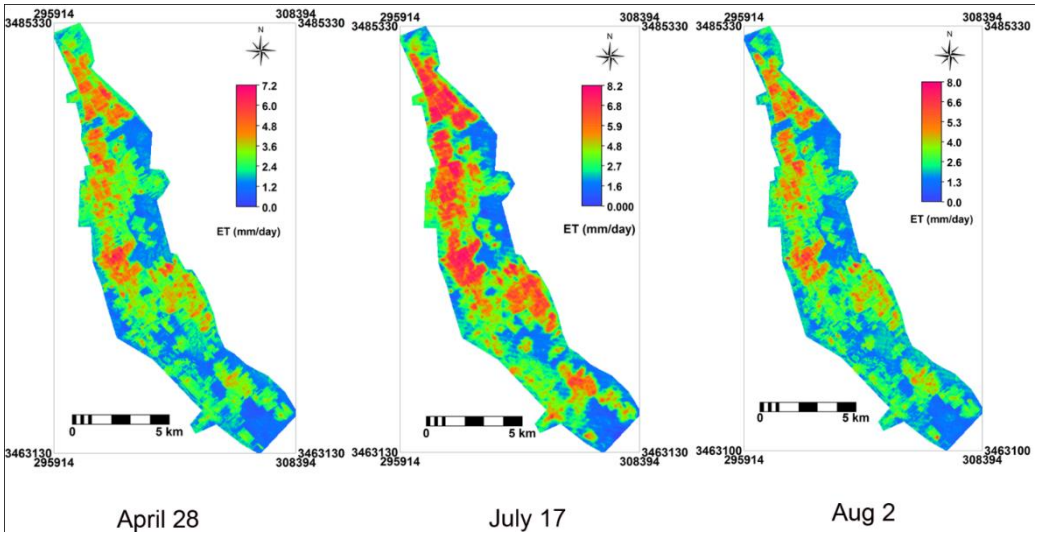

Fig. 6- Maps showing spatial distribution of ET over the pistachio crop on three different dates

Table 1- Hourly and daily reference ET (ASCE Penman-Monteith method) and wind speed

April 28				July 17				Aug 2			
ET reference		U_4 * (m/s)		ET reference		U_4 * (m/s)		ET reference		U_4* (m/s)	
Hourly	Daily	Hourly	Daily	Hourly	Daily	Hourly	Daily	Hourly	Daily	Hourly	Daily
0.79	8.4	2	2.33	0.87	8.43	1	0.6	0.7	7.62	2.9	4.3

*U_4 is the wind speed at the 4 m above ground.

Table 2- ET values (mm) at three LAI level

Pistachio crop		Day of 118	Day of 198	Day of 214
		Estimated	Estimated	Estimated
LAI 2-3	S1	3.3	6.6	4.5
	S2	3.2	5.3	3.8
	S3	2.9	4.6	3.4
	S4	3.0	4.6	3.7
LAI 3-4	S1	4.8	6.6	5.7
	S2	4.4	6.8	5.7
	S3	4.4	6.7	5.1
	S4	4.9	6.6	5.0
LAI 4-5	S1	6.3	7.8	6.6
	S2	6.9	7.9	6.9
	S3	6.2	7.9	7.3
	S4	5.7	7.6	6.6

*S1-S4 are the number of samples in each LAI category

4. Conclusion

The existence of numerous and different algorithms and methods for estimating evapotranspiration using satellite images as well as the production of new methods, some of which are very different from previous algorithms, show that remote sensing technology, although rapidly evolving, still has a long way to go. Has a leader. Therefore, it is necessary to carefully examine the existing methods and to present newer methods with better estimation accuracy.

In general, the use of remote sensing techniques and the METRIC algorithm as a new method for estimating evapotranspiration have appropriate. In this study, three LandsatTM 5 images obtained on April 28, July 17 and August 2, 2010 were used to estimate ET through METRIC. METRIC estimates the average ET for the image on April 28, July 17 and August 2 at 2.9, 4.2 and 3.1 mm per day, respectively. The results showed that this algorithm is very sensitive to the parameters of surface temperature, NDVI index and sensible heat flux and the estimation of daily evapotranspiration using the metric algorithm depends on the accuracy of estimation of these three parameters. Which is

consistent with the (Reyes-González etal., 2019; Mokhtari etal., 2012; Ghane Ezabadi et al. 2021) results .

Funding Information (Private funding by authors, or funding's ID)

Conflict of Interest /Competing interests (None)

Availability of Data and Material (Data are available when requested)

Code availability (Not applicable)

REFERENCES

Allen, R. G., Pereira, L. S., Raes, D., & Smith, M. (1998). Crop evapotranspiration-Guidelines for computing crop water requirements-FAO Irrigation and drainage paper 56. *Fao, Rome*, *300*(9), D05109.

Allen, R. G., Tasumi, M., & Trezza, R. (2007). Satellite-based energy balance for mapping evapotranspiration with internalized calibration (METRIC)—Model. *Journal of irrigation and drainage engineering*, *133*(4), 380-394. https://doi.org/10.1061/(ASCE)0733-9437(2007)133:4(395)

Allen, R. G., Tasumi, M., Morse, A., & Trezza, R. (2005). A Landsat-based energy balance and evapotranspiration model in Western US water rights regulation and planning. *Irrigation and Drainage systems*, *19*(3-4), 251-268. https://doi.org/10.1007/s10795-005-5187-z

Allen, R. G., Tasumi, M., Morse, A., & Trezza, R. (2005). Satellite-based evapotranspiration by energy balance for western states water management. In *Impacts of Global Climate Change* (pp. 1-18). https://doi.org/10.1061/40792(173)556

Barreto, Á., Arbelo, M., Hernández-Leal, P. A., Núñez-Casillas, L., Mira, M., & Coll, C. (2010). Evaluation of surface temperature and emissivity derived from ASTER data: A case study using ground-based measurements at a volcanic site. *Journal of Atmospheric and Oceanic Technology*, *27*(10), 1677-1688. https://doi.org/10.1175/2010JTECHA1447.1

Bastiaanssen, W. G. (2000). SEBAL-based sensible and latent heat fluxes in the irrigated Gediz Basin, Turkey. *Journal of hydrology*, *229*(1-2), 87-100. https://doi.org/10.1016/S0022-1694(99)00202-4

Bastiaanssen, W. G., Menenti, M., Feddes, R. A., & Holtslag, A. A. M. (1998). A remote sensing surface energy balance algorithm for land (SEBAL). 1. Formulation. *Journal of hydrology*, *212*, 198-212. https://doi.org/10.1016/S0022-1694(98)00253-4

Bastiaanssen, W. G., Molden, D. J., & Makin, I. W. (2000). Remote sensing for irrigated agriculture: examples from research and possible applications. *Agricultural water management*, *46*(2), 137-155. https://doi.org/10.1016/S0378-3774(00)00080-9

Brutsaert, W. (1982). Evaporation into the atmosphere: Theory. *History, and Applications*, *1*. https://doi.org/10.1007/978-94-017-1497-6

Choi, M., Kustas, W. P., Anderson, M. C., Allen, R. G., Li, F., & Kjaersgaard, J. H. (2009). An intercomparison of three remote sensing-based surface energy balance algorithms over a corn and soybean production region (Iowa, US) during SMACEX. *Agricultural and Forest Meteorology*, *149*(12), 2082-2097. https://doi.org/10.1016/j.agrformet.2009.07.002

Folhes, M. T., Rennó, C. D., & Soares, J. V. (2009). Remote sensing for irrigation water management in the semi-arid Northeast of Brazil. *Agricultural Water Management*, *96*(10), 1398-1408. https://doi.org/10.1016/j.agwat.2009.04.021

Gao, Y., & Long, D. (2008). Intercomparison of remote sensing-based models for estimation of evapotranspiration and accuracy assessment based on SWAT. *Hydrological Processes: An International Journal*, *22*(25), 4850-4869. https://doi.org/10.1002/hyp.7104

Ghane Ezabadi, N., Azhdar, S., & Jamali, A. A. (2021). Analysis of dust changes using satellite images in Giovanni NASA and Sentinel in Google Earth Engine in western Iran. *Journal of Nature and Spatial Sciences (JONASS)*, *1*(1), 17-26.

Gowda, P. H., Chavez, J. L., Colaizzi, P. D., Evett, S. R., Howell, T. A., & Tolk, J. A. (2008). ET mapping for agricultural water management: present status and challenges. *Irrigation science*, *26*(3), 223-237. https://doi.org/10.1007/s00271-007-0088-6

Gowda, P. H., Chavez, J. L., Colaizzi, P. D., Evett, S. R., Howell, T. A., & Tolk, J. A. (2007). Remote sensing based energy balance algorithms for mapping ET: Current status and future challenges. *Transactions of the ASABE*, *50*(5), 1639-1644. https://doi.org/10.13031/2013.23964

Gowda, P. H., Chávez, J. L., Howell, T. A., Marek, T. H., & New, L. L. (2008). Surface energy balance based evapotranspiration mapping in the Texas high plains. *Sensors*, *8*(8), 5186-5201. https://doi.org/10.3390/s8085186

Jain, S. K., Nayak, P. C., & Sudheer, K. P. (2008). Models for estimating evapotranspiration using artificial neural networks, and their physical interpretation. *Hydrological Processes: An International Journal*, *22*(13), 2225-2234. https://doi.org/10.1002/hyp.6819

Jamali, A. A., & Ghorbani Kalkhajeh, R. (2020). Spatial Modeling Considering valley's Shape and Rural Satisfaction in Check Dams Site Selection and Water Harvesting in the Watershed. *Water Resources Management*, *34*(10), 3331-3344.

Jamali, A. A., Tabatabaee, R., & Randhir, T. O. (2021). Ecotourism and socioeconomic strategies for Khansar River watershed of Iran. *Environment, Development and Sustainability*, 1-17.

Liaqat, U. W., & Choi, M. (2015). Surface energy fluxes in the Northeast Asia ecosystem: SEBS and METRIC models using

Landsat satellite images. *Agricultural and Forest Meteorology*, *214*, 60-79. https://doi.org/10.1016/j.agrformet.2015.08.245

Mokhtari, M. H., Ahmad, B., Hoveidi, H., & Busu, I. (2013). Sensitivity analysis of METRIC–based evapotranspiration algorithm. https://doi.org/10.22059/IJER.2013.620

Muukkonen, P., & Heiskanen, J. (2005). Estimating biomass for boreal forests using ASTER satellite data combined with standwise forest inventory data. *Remote sensing of Environment*, *99*(4), 434-447. https://doi.org/10.1016/j.rse.2005.09.011

Norman, J. M., Kustas, W. P., & Humes, K. S. (1995). Source approach for estimating soil and vegetation energy fluxes in observations of directional radiometric surface temperature. *Agricultural and Forest Meteorology*, *77*(3-4), 263-293. https://doi.org/10.1016/0168-1923(95)02265-Y

Pôças, I., Paco, T. A., Cunha, M., Andrade, J. A., Silvestre, J., Sousa, A., ... & Allen, R. G. (2014). Satellite-based evapotranspiration of a super-intensive olive orchard: Application of METRIC algorithms. *Biosystems Engineering*, *128*, 69-81. https://doi.org/10.1016/j.biosystemseng.2014.06.019

Qanbari, V., & Jamali, A. A. (2015). The relationship between elevation, soil properties and vegetation cover in the Shorb-Ol-Ain watershed of Yazd. *J Biodivers Environ Sci (JBES)*, 49-56.

Rahimian, M. H., Shayannejad, M., Eslamian, S., Gheysari, M., & Jafari, R. (2017). SEBAL application to estimate water use efficiency of Pistachio trees in saline condition (Case study: Bahadoran Plain, Iran). *Journal. Bio. Env. Sci.* 10(6), 248-257. https://www.innspub.net.

Ramírez-Cuesta, J. M., Allen, R. G., Intrigliolo, D. S., Kilic, A., Robison, C. W., Trezza, R., ... & Lorite, I. J. (2020). METRIC-GIS: An advanced energy balance model for computing crop evapotranspiration in a GIS environment. *Environmental Modelling & Software*, *131*, 104770. https://doi.org/10.1016/j.envsoft.2020.104770

Ramos, J. G., Cratchley, C. R., Kay, J. A., Casterad, M. A., Martínez-Cob, A., & Dominguez, R. (2009). Evaluation of satellite evapotranspiration estimates using ground-meteorological data available for the Flumen District into the Ebro Valley of NE Spain. *Agricultural water management*, *96*(4), 638-652. https://doi.org/10.1016/j.agwat.2008.10.001

Reyes-González, A., Kjaersgaard, J., Trooien, T., Reta-Sánchez, D. G., Sánchez-Duarte, J. I., Preciado-Rangel, P., & Fortis-Hernández, M. (2019). Comparison of leaf area index, surface temperature, and actual evapotranspiration estimated using the METRIC model and in situ measurements. *Sensors*, *19*(8), 1857. https://doi.org/10.3390/s19081857

Roerink, G. J., Su, Z., & Menenti, M. (2000). S-SEBI: A simple remote sensing algorithm to estimate the surface energy balance. *Physics and Chemistry of the Earth, Part B: Hydrology, Oceans and Atmosphere*, *25*(2), 147-157. https://doi.org/10.1016/S1464-1909(99)00128-8

Su, Z. (2002). The Surface Energy Balance System (SEBS) for estimation of turbulent heat fluxes. Hydrology and Earth System Sciences 6(1): 85-100. https://doi.org/10.5194/hess-6-85-2002, 2002. https://doi.org/10.5194/hess-6-85-2002

Tasumi, M. (2019). Estimating evapotranspiration using METRIC model and Landsat data for better understandings of regional hydrology in the western Urmia Lake Basin. *Agricultural Water Management*, *226*, 105805. https://doi.org/10.1016/j.agwat.2019.105805

Tasumi, M., Trezza, R., Allen, R. G., & Wright, J. L. (2005). Operational aspects of satellite-based energy balance models for irrigated crops in the semi-arid US. *Irrigation and Drainage Systems*, *19*(3-4), 355-376. https://doi.org/10.1007/s10795-005-8138-9

Ye, X., Zhang, Q., Liu, J., Li, X., & Xu, C. Y. (2013). Distinguishing the relative impacts of climate change and human activities on variation of streamflow in the Poyang Lake catchment, China. *Journal of Hydrology*, *494*, 83-95. https://doi.org/10.1016/j.jhydrol.2020.124883